Inorganic Chemistry
Cite This: Inorg. Chem. 2019, 58, 2610−2617
Article
pubs.acs.org/IC

Hexagonal Bipyramidal Dy(III) Complexes as a Structural Archetype for Single-Molecule Magnets

Jing Li,[†] Silvia Gómez-Coca,[§,∥] Brian S. Dolinar,[§] Li Yang,[†] Fei Yu,[†] Ming Kong,[†] Yi-Quan Zhang,*[,‡] You Song,*[,†] and Kim R. Dunbar*[,§]

[§]Department of Chemistry, Texas A&M University, P.O. Box 30012, College Station, Texas 77842, United States
[†]State Key Laboratory of Coordination Chemistry, School of Chemistry and Chemical Engineering, Nanjing University and [‡]Jiangsu Key Laboratory for NSLSCS, School of Physical Science and Technology, Normal University, Nanjing 210023, PR China
[∥]Department of Chemistry, King's College London, London SE1 1DB, United Kingdom

Supporting Information

ABSTRACT: Single-molecule magnets (SMMs), are regarded as excellent nanomaterials for high-density information storage and quantum computing. The local symmetry of the crystal field for the metal ion plays an important role in pursuing a high-performance SMM. Herein, two highly stable distorted hexagonal bipyramidal (quasi-D_{6h}) Dy complexes exhibiting slow relaxation of the magnetization are reported. A hexagonal bipyramidal Dy model complex with 18-crown-6 was also designed to study the relationship between magnetic anisotropy and symmetry. The combined experimental and theoretical results indicate that quantum tunneling is highly dependent on the local symmetries of the crystal field. The magnetic anisotropy becomes much stronger when the symmetry is closer to a standard D_{6h} geometry. These results support the conclusion that the hexagonal bipyramidal geometry is a viable one for the design of new classes of SMMs.

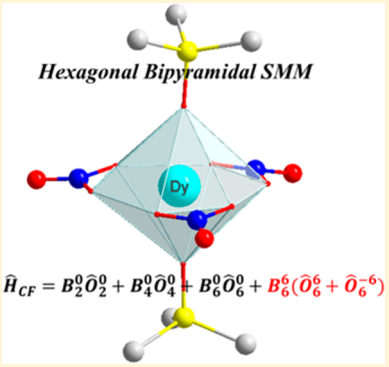

INTRODUCTION

Single-molecule magnets (SMMs), molecules that exhibit slow magnetic relaxation and magnetic hysteresis of a molecular origin, were first reported in 1993.[1] Their potential for applications in high-density information storage[2] and quantum computing devices[3] has sparked a new field of coordination chemistry aimed at the synthesis of transition metal- and lanthanide-based SMMs. Since the well-known dodecametallic manganese-acetate complex $[Mn_{12}O_{12}(OAc)_{16}(H_2O)_4]$-($Mn_{12}Ac$) was reported,[1,4] hundreds of polynuclear transition metal compounds have been synthesized as targets for nanoscale magnets.[5] As a result of these efforts, many fascinating cases of large ground spin states or high anisotropies in the form of negative axial zero-field splitting (D) have been unearthed.[6] The combination of both desired properties, however, is difficult to accomplish. Polynuclear SMMs with strongly coupled metal spins can give rise to a high total spin ground state S, but the geometries of such molecules are more symmetric than single metal ion complexes which reduces the magnetic anisotropy of molecules.[7] Simply put, the S values and negative D values are countervailing trends.

Mononuclear SMMs with very large anisotropies have become prominent in the field of molecular magnetism in recent years. Lanthanide ions such as Tb(III),[8] Dy(III)[9] and Er(III)[10] exhibit relatively large spin ground states and huge spin−orbit coupling effects. Many mononuclear SMMs have been designed based on the aforementioned lanthanide ions as well as low coordinate first row transition metal complexes.[11,12]

Quantum tunneling of the magnetization (QTM) constitutes another major challenge for designing SMMs.[13] A considerable body of theoretical calculations and experimental data has led to a general understanding that QTM is caused by the overlap of wave functions[13] and is strongly influenced by crystal fields,[14] inter- and intramolecular interactions,[15] and hyperfine interactions.[16] Unlike polynuclear systems, QTM of mononuclear SMMs cannot be avoided through coupling interactions in order to ameliorate fast relaxation.[15] Consequently, an approach that serves to exert control over the crystal field is the logical choice. The crystal-field effect can be described by the Hamiltonian $\hat{H}_{CF} = \sum B_k^q \hat{O}_k^q$[17a] ($B_k^q$ are crystal field parameters and $\hat{O}_k^q$ are the equivalent operators in Stevens notation).[17b,c] Usually the elements with $q \neq 0$ and $k = 2, 4$ (and 6 for lanthanide ions) are considered to be one of the sources of QTM. Some local symmetries of the crystal field, such as $D_{\infty h}$ for linear 2-coordinate,[18] D_{5h} for pentagonal bipyramidal,[9a−c] D_{4d} for square antiprismatic,[8b,19] and sandwich-type,[10a,c] complexes, are known to mitigate QTM.

An ideal hexagonal bipyramid (D_{6h}) with the crystal field Hamiltonian $\hat{H}_{CF} = B_2^0\hat{O}_2^0 + B_4^0\hat{O}_4^0 + B_6^0\hat{O}_6^0 + B_6^6(\hat{O}_6^6 + \hat{O}_6^{-6})$ might also serve as an appropriate symmetry for mononuclear SMMs,[20] because B_k^q ($q \neq 0$, and $k = 2, 4, 6$) vanishes except for B_6^6 in this symmetry for the crystal field, which can weaken the QTM in theory.[17a] On the basis of this hypothesis, we

Received: November 16, 2018
Published: January 29, 2019

DOI: 10.1021/acs.inorgchem.8b03206
Inorg. Chem. 2019, 58, 2610−2617

report slow magnetic relaxation behavior in the distorted hexagonal bipyramidal Dy-based complexes $[Dy(t\text{-}Bu_3PO)_2(NO_3)_3]$ (**1**) and $[Dy(t\text{-}Bu_3PO)_2(NO_3)_3]\cdot 0.5CH_3CN$ (**2**). Their magnetic properties have been measured and elucidated through crystal field and ab initio calculations.

RESULTS AND DISCUSSION

Crystal Structures. Complex **1** was synthesized in EtOH according to a literature procedure,[21] and **2** was synthesized in CH_3CN. Both complexes self-assemble from Dy(III) ions, *t*-Bu_3PO ligands, and NO_3^- and are stable in air. When the solutions of metal ion and ligands are mixed, white crystals immediately appear. Interestingly, they share a similar $[Dy(t\text{-}Bu_3PO)_2(NO_3)_3]$ unit (Figure 1), that are different morphologies or different solvates than the structure reported in ref 21.

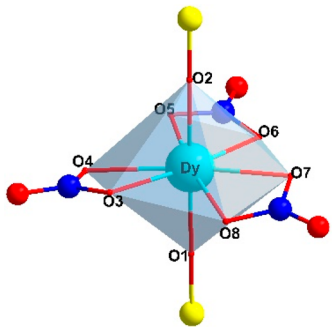

Figure 1. Local structures of complexes **1** and **2**. H and C atoms are omitted for the sake of clarity. Color code: N, blue; O, red; P, yellow; Dy, cyan.

Complex **1** crystallizes in the orthorhombic space group *P*nma (Table S1), with one-half of a molecule of **1** in the asymmetric unit. The molecule lies on a crystallographic mirror plane (Figures 1 and S2). The *t*-Bu_3PO groups occupy the axial positions and the three chelating nitrate anions occupy the equatorial positions and are coplanar. The Dy(III) ion is in the plane of the nitrate ligands, deviating only 0.07(6) Å from the equatorial plane. The equatorial Dy−O distances are 2.375(7)−2.416(9) Å longer than the axial ones of 2.213(7) and 2.215(7) Å, indicating that the coordination environment of Dy(III) is a compressed distorted hexagonal bipyramid (Continuous Shape Measurement[22] relative to the hexagonal bipyramid, CShM(HBPY), of 0.636). The axial *t*-Bu_3PO groups form a nearly linear O1−Dy−O2 angle of 172.6(3)°. The O−Dy−O bite angles of the nitrate ions range from 52.1(3) to 56.2(4)°, and the O−Dy−O bond angles between nitrate ions range from 64.8(3) to 69.8(5)° (Figure S2 and Table S2). Furthermore, the distance between adjacent oxygen atoms of the same nitrate ion range from 2.09(6) to 2.27(5) and between nitrate ions range from 2.58(0) to 2.71(9) Å (Figure S2). The complexes pack the unit cell along the *n* and *a* glide planes of the space group, resulting in intermolecular Dy···Dy distances of 9.29(1) Å (nearest neighbors) and 10.914(8) Å (next nearest neighbors) (Figure S1).

Complex **2** crystallizes in the monoclinic space group $P2_1/c$ with two independent molecules of $Dy(NO_3)_3(t\text{-}Bu_3PO)_2$ in the asymmetric unit (**2-A** and **2-B**). These molecules exhibit slightly different geometries than that of complex **1**. Two of the chelated nitrate ions are rotated about the N···Dy axis by approximately 10−15° which breaks the symmetry of the nitrate ligand plane that was observed for **1**. As a result of these rotations, the coordination geometry of **2-A** and **2-B** are more distorted from that of an ideal hexagonal bipyramid than is **1** (CShM = 1.108 and 1.237, respectively). The shortest distance between Dy(III) ions of neighboring units is 8.47(1) Å, which is shorter than that found in **1** (Figure S1). The average Dy−O bond lengths and O−Dy−O angles are summarized in Table S2.

Static Magnetic Properties. The temperature-dependent direct-current (dc) magnetic susceptibility measurements (Figure S3) were performed under a 1 kOe applied dc field on polycrystalline samples of **1** and **2**. The room temperature $\chi_M T$ values are 14.16 $cm^3\ mol^{-1}\ K$ (**1**) and 14.2 $cm^3\ mol^{-1}\ K$ (**2**), which are in good agreement with the expected values (S = 5/2, L = 5, $^6H_{15/2}$, J = 15/2, g_J = 4/3, 14.17 $cm^3\ mol^{-1}\ K$). The $\chi_M T$ products decrease gradually over the whole temperature range for both complexes, an indication of the thermal depopulation of the excited m_J states of the Dy(III) ions and anisotropies of the Dy(III) ions. The magnetization data of **1** and **2** from zero dc field to 7 T at different temperatures are depicted in Figure S3 (inset). All field-dependent magnetizations at 1.8 K exhibit an abrupt increase below 1 T, and the slight increase reaching the maximum magnetizations of approximately 5 Nμ_B without saturation, indicating strong magnetic anisotropy of Dy(III) ions.[9,19]

A small hysteresis loop was observed for **1** at 1.8 K, indicating strong QTM for **1**. Complex **2** exhibits typical butterfly-shaped loops at low temperature due to the faster relaxation at zero field and becoming slower in the presence of a field (Figure S4). The hysteresis loops remain open up to at least 3 K for **2**.

Dynamic Magnetic Properties. In order to probe the low-temperature relaxation dynamics of the two complexes, temperature and frequency dependence of the alternating current (ac) magnetic susceptibility measurements were carried out on polycrystalline samples (Figures S5, S6, S9, and S10). Under a zero applied dc field, only the beginning of temperature dependent out-of-phase ac susceptibility signals indicating slow relaxation of the magnetization was apparent for **1** and **2** (Figures S6 and S10). The peak is largely temperature independent which is consistent with quantum tunneling of the magnetization. To further evaluate the magnetic properties, we examined the ac magnetic susceptibility properties while applying an external magnetic field to suppress QTM. The field dependence of the ac susceptibility data was examined between 0.2 and 3 kOe (Figures S5 and S9); these are sufficiently small fields such that the influence of Zeeman effects can be ignored.

Although there are two symmetry-independent molecules in **2**, only one relaxation process was observed over the whole field range. The field of 0.8 kOe was chosen as optimal for the observation of a maximum in χ_M'' for the two complexes. In order to study the influence of magnetic field for magnetization dynamic properties, a 2.0 kOe external dc field was also applied to perform additional ac measurements over the same temperature range.

Under a 0.8 kOe external dc field, frequency-dependence of the in-phase (χ_M') and out-of-phase (χ_M'') ac susceptibility data exhibit typical slow magnetic relaxation behavior (Figures 2a,b, S7a, and S11a). Only one slow relaxation process was observed over the entire temperature range. The maximum for χ_M'' (999 Hz) appears at 8.8 and 10.1 K for **1** and **2**,

DOI: 10.1021/acs.inorgchem.8b03206
Inorg. Chem. 2019, 58, 2610−2617

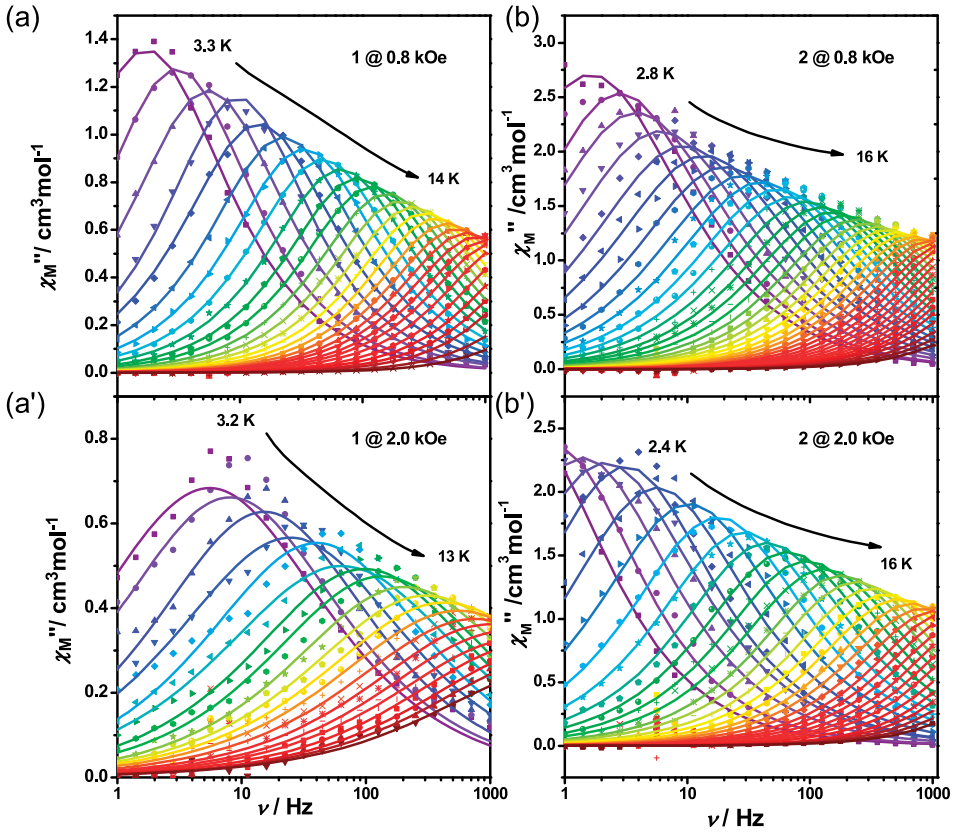

Figure 2. Out-of-phase alternating-current molar magnetic susceptibilities for **1** under 0.8 kOe (a) and 2.0 kOe (a′), for **2** under 0.8 kOe (b) and 2.0 kOe (b′) dc field. Lines are the fitting results.

Table 1. Fitting Results for Complexes 1 and 2 under 0.8 and 2.0 kOe dc Field with Arrhenius Law and eq 1

complex	1				2			
dc field	0.8 kOe		2.0 kOe		0.8 kOe		2.0 kOe	
model	Arr. Law	eq 1	Arr. Law	eq 1	Arr. Law	eq 1	Arr. Law	eq 1
A (s^{-1} K^{-1})		1.44		1.00		0		2.24
C (s^{-1} K^{-1})		0.0055		0.0036		0.0013		0.0018
n		6.00		6.00		5.80		5.80
τ_0 (s)	2.72×10^{-6}	6.23×10^{-6}	3.37×10^{-6}	5.02×10^{-6}	2.01×10^{-6}	3.64×10^{-6}	2.93×10^{-6}	3.76×10^{-6}
U_{eff} (K)	38.4	37.1	36.9	36.5	48.3	46.9	43.5	43.8

respectively. There is still only one relaxation process for both complexes under 2.0 kOe (Figures 2a′,b′, S7b, and S11b).

The relaxation times (τ) were extracted from the ac susceptibilities susceptibilities using a generalized Debye model[23] with CCFIT package. The coefficient α is 0−0.17 in the 3.3−14 K range for **1** (Table S4 and Figure S8a), and 0−0.15 in the 4−16 K temperature range for **2** (Table S6 and Figure S12a) under 0.8 kOe, which is indicative of a relatively narrow distribution of relaxation times. The Cole−Cole fitting results for the 2.0 kOe data are essentially the same; these are summarized in Figures S8b and S12b and Tables S5 and S7.

In the high-temperature region, $\ln(\tau)$ is linearly dependent on T, indicative of a thermal relaxation process. The best fit to the Arrhenius law is summarized in Table 1 (plots shown in Figure 3). The energy barrier is ~36.9−38.4 K for **1**, which is lower than the one for **2** (43.5−48.3 K). In the low temperature regime, $\ln(\tau)$ exhibits a nonlinear dependence on T, presumably due to the presence of nonthermal relaxation pathways. In this case, the relaxation data may have contributions from QTM, direct, Raman, and Orbach relaxation processes.[24] No obvious QTM process can be ascertained from the frequency-dependent out-of-phase ac susceptibility data, so to avoid overparameterization, the QTM process was ignored in the fits. The fitting is described in the following:

$$\tau^{-1} = AT + CT^{n} + \tau_0^{-1} \exp(-U/k_B T) \quad (1)$$

where A is the direct coefficient, C and n are the Raman coefficients, H is the magnetic field, U is the thermal barrier of the Orbach relaxation process, T is temperature, and k_B is the Boltzmann constant.

The Raman process is typically regarded as a magnetic field independent process. The coefficient n is fixed for fitting the high magnetic field data. The best fits were obtained with an n = 6.00 for **1** and n = 5.80 for **2**. Although the parameter n in the Raman relaxation process is usually equal to 9 for Kramers ions,[25] lower values may be expected if optical phonons are taken into account.[24] The thermal barrier of the Orbach relaxation process is similar to the linear fittings. For complex **2**, the direct process is sensitive to the magnetic field; at high

DOI: 10.1021/acs.inorgchem.8b03206
Inorg. Chem. 2019, 58, 2610−2617

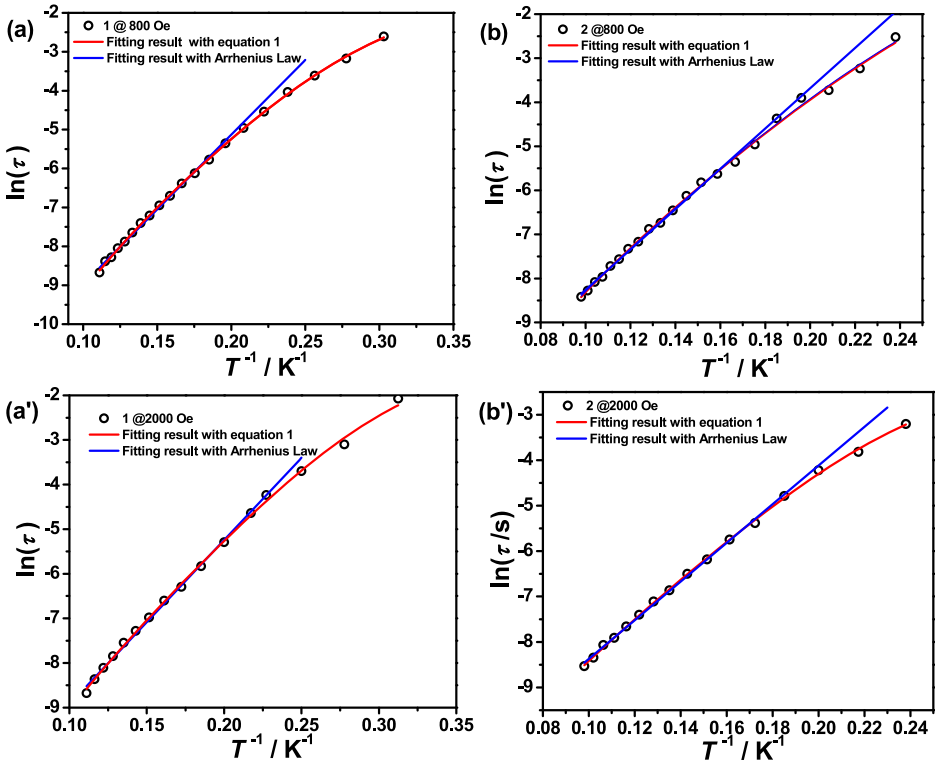

Figure 3. Arrhenius plots of ln(τ) vs the inverse temperature T^{-1}, calculated from data at dc field of 0.8 kOe (a) and 2.0 kOe (a′) for **1**; 0.8 kOe (b) and 2.0 kOe (b′) for **2**, respectively. Blue lines show the fit of data to the Arrhenius expression $\tau = \tau_0 \exp(U_{eff}/k_B T)$, and red lines show the fit of data using eq 1, see in the text. For parameters of the fit, see Table S7.

temperatures, the Orbach process is dominant. As the temperature is lowered, the Raman process begins to play an important role in the relaxation process (Figure 3).

Theoretical Analysis. Complete Active Space Self-Consistent Field (CASSCF) calculations on the Dy fragments of complexes **1**, **2-A**, and **2-B**, using X-ray crystal structure parameters (Figure S14) were carried out with the MOLCAS 8.2 program package.[26] Complexes **2-A** and **2-B** have a quasi-C_3 and three quasi-C_2 symmetry axes, while **1** has a quasi-C_3 and only one C_2 axis. The calculations predict that the ground states of complexes **2-A** and **2-B** are well-separated from the first excited states (162.9 and 168.8 cm^{-1}, respectively, Table S8) with strong magnetic anisotropy of the ground state (J = 15/2, $g_{x,y} \approx 10^{-3}$). A much lower degree of magnetic axiality in the ground state was found for complex **1** ($g_{x,y} \approx 10^{-1}$) (Table 2). The orientation of the main magnetic axis of the ground Kramers doublet in **1** is oriented in the equatorial plane, while the anisotropy axes of **2-A** and **2-B** coincide with the geometric C_3 axis (Figure S14), indicating that the magnetic anisotropy is sensitive to the local symmetry. The matrix elements of the transversal magnetic moment between states[27] which is related to the rate of spin-phonon transitions and the degree of QTM, is described in detail in Figure 4. The electronic states and magnetic transition probabilities for the complexes in zero field give the most probable relaxation paths where the values of the transverse magnetic moment are the largest. In this way the corresponding blocking barrier can be defined.[28]

For **1**, the transverse magnetic moment is non-negligible in the ground state (0.19 μ_B), which explains why QTM is fast at low temperature which is in good agreement with the fact that there is only a weak ac susceptibility response in zero external field. The relaxation path (|−15/2⟩→ |−5/2⟩ → |+5/2⟩ → |+15/2⟩) which is defined as thermally assisted QTM is another possibility. With an external dc field, the QTM within the ground doublets is suppressed, resulting in a field-induced

Table 2. g (g_x, g_y, g_z) Tensors of the Lowest Kramers Doublets (KDs) of the Dy Fragments of Complexes 1, 2-A, 2-B, and Model Complex

KDs		1	2-A	2-B	model
1	g_x	0.455	0.002	0.001	0.000
	g_y	0.703	0.011	0.019	0.000
	g_z	17.900	19.601	19.610	19.893
2	g_x	9.026	10.447	9.860	0.089
	g_y	8.387	8.365	8.624	0.091
	g_z	2.598	3.457	3.785	17.028
3	g_x	10.467	0.608	0.781	0.068
	g_y	7.573	1.102	1.250	0.131
	g_z	1.649	2.590	2.232	13.937
4	g_x	9.408	9.366	8.098	1.211
	g_y	7.183	6.413	6.702	1.976
	g_z	4.126	3.056	3.979	7.524
5	g_x	1.965	1.161	0.332	0.033
	g_y	3.569	1.734	1.539	2.037
	g_z	6.875	6.584	5.225	9.917
6	g_x	2.487	1.779	10.356	0.016
	g_y	4.859	5.295	5.870	3.784
	g_z	9.178	9.597	0.426	9.898
7	g_x	2.501	1.846	1.703	0.023
	g_y	2.613	6.379	5.478	0.574
	g_z	12.634	12.650	10.278	5.505
8	g_x	0.001	0.702	11.763	12.315
	g_y	0.504	3.015	7.974	7.226
	g_z	16.258	15.317	1.956	1.207

DOI: 10.1021/acs.inorgchem.8b03206
Inorg. Chem. 2019, 58, 2610−2617

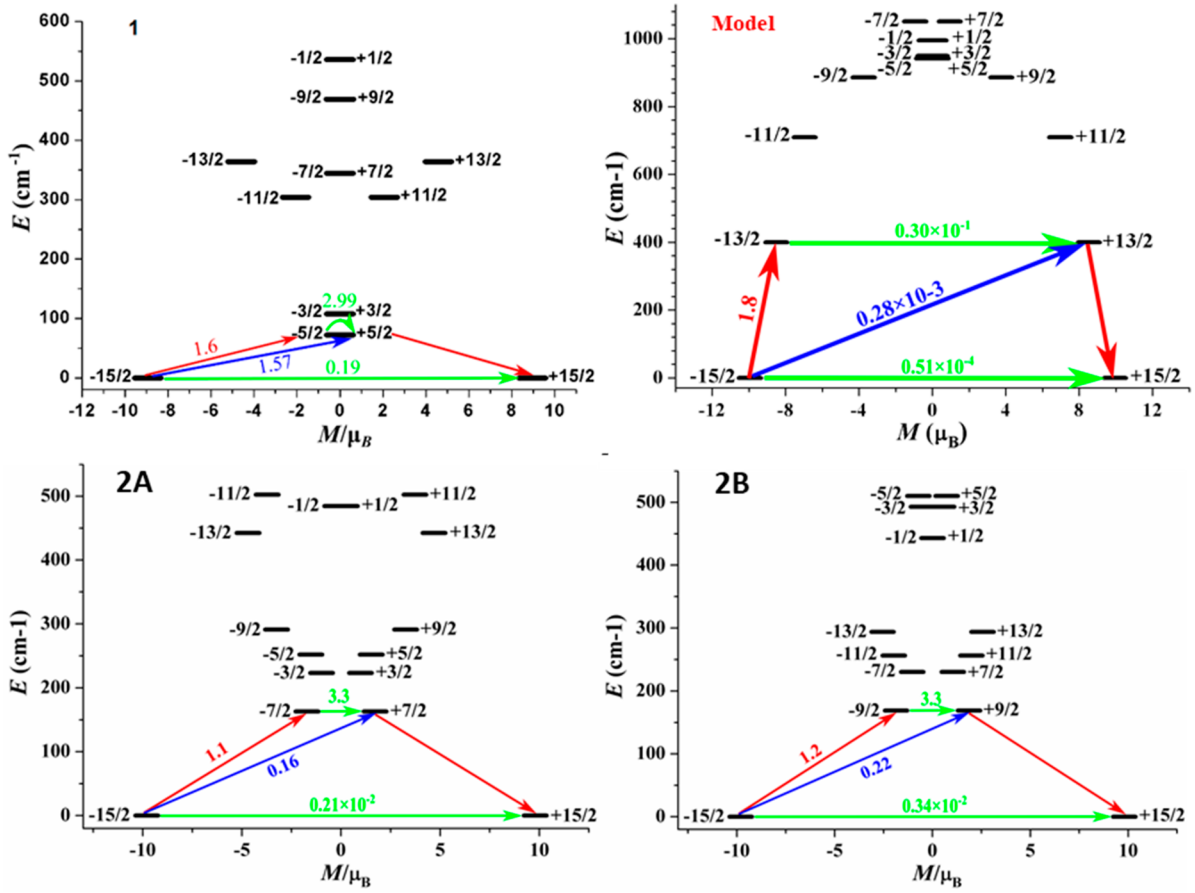

Figure 4. Magnetization blocking barriers in **1** and model complex **2-A**, and **2-B**. The thick black lines represent the Kramers doublets as a function of their magnetic moment along the magnetic axis. The green lines correspond to diagonal quantum tunnelling of the magnetization (QTM); the blue line represents off-diagonal relaxation process. The numbers at each arrow refer to the mean absolute value of the corresponding matrix element of transition magnetic moment.

SMM. The most possible relaxation routes for **2** are thermally assisted QTM though the first excited states (J = 7/2 for **2-A** and J = 9/2 for **2-B**) with a small transverse magnetic moment in the ground state (ca. 10^{-2} μ_B). From theoretical calculation only, both complexes might be SMMs with high energy barriers.

To understand the underlying origin of different dynamic magnetic properties for **1** and **2**, we analyzed the parameters of the crystal field for these complexes from the MOLCAS 8.2 calculation results. (Table S9). For an ideal hexagonal bipyramid, the crystal field Hamiltonian is defined by $\hat{H}_{CF} = B_2^0\hat{O}_2^0 + B_4^0\hat{O}_4^0 + B_6^0\hat{O}_6^0 + B_6^6(\hat{O}_6^6 + \hat{O}_6^{-6})$.[15a]

Distortions in the geometry, however, make the equivalent operators $\hat{O}_k^q$ with $q \neq 0$ relevant. The parameters B_n^0 (n = 2, 4, 6) and B_6^6 are larger than other parameters for complexes **1** and **2**, which is in good agreement with the D_{6h} symmetry crystal field Hamiltonian. The nonzero values of B_n^m(n = 2, 4, $-n \leq m \leq n$, and $m \neq 0$) suggests significant QTM in the absence of an external dc field for all complexes. For complex **1**, the axial parameter B_2^0 (−1.56) is equal in magnitude to the nonaxial parameter B_2^2 (1.50), accounting for its poor SMM performance under a zero dc field. The axial parameter B_2^0 of complexes **2-A** and **2-B** is 10 times larger than other nonaxial parameters, suggesting a stronger uniaxial anisotropy. As a result, a high-temperature hysteresis loop is observed.

The calculated energy gaps between the ground and the first excited states for the three complexes (Table S9) are much larger than the experimental ones, an indication that the Orbach process is not the primary relaxation route. It has been recently shown[9d,29] that low energy intramolecular vibrations play an important role in spin relaxation of SMMs. In the current work, the experimental energy barriers of **1** and **2** are very similar and close to 40 K, which are consistent with the typical energies of low energy vibration modes.[29c] The molecules in **1**, **2-A**, and **2-B** have the same chemical composition and similar geometries; therefore, the local vibrations should be very similar. In fact, the very different theoretical energy barriers and similar experimental energy barriers suggest that the low energy vibrations are contributing to relaxation of the spin in a similar fashion.

Both **1** and **2** exhibit poor SMM performance so it is not possible to discern on the basis of these data alone whether the hexagonal bipyramidal geometry is a viable one for the design of new classes of SMMs with high performance. Clearly, it is possible that the magnetic properties are related primarly to the symmetry distortion. To test this hypothesis, a more standard hexagonal bipyramidal Dy model complex with 18-crown-6 and Me_3PO was designed (Figure S13 and Table S8). The calculated results based on this model are summarized in Tables 2, S9, and S11. The calculations indicate that the three lowest doublets of the model complex have very strong magnetic anisotropy: g_x = g_y = 0.000, and g_z = 19.893 for the ground state (J = 15/2); g_x = 0.089, g_y = 0.091, g_z = 17.028 for the first excited state (J = 13/2); g_x = 0.068, g_y = 0.131, and g_z

DOI: 10.1021/acs.inorgchem.8b03206
Inorg. Chem. 2019, 58, 2610−2617

= 13.937 for the second excited state (J = 11/2). The wave functions with a projection of the total moment $|m_J\rangle$ for the lowest three spin−orbit states are quite pure. The most possible relaxation routes for model complex are thermally assisted QTM though the first excited states with a very small transverse magnetic moment in the ground state (ca. 10^{-4} μ_B, Figure 4). All of these findings indicate that the magnetic anisotropy become stronger when the symmetry is closer to D_{6h}. The results indicate that the hexagonal bipyramidal geometry is a viable one for the design of new classes of SMMs.

CONCLUSIONS

In the present work, two highly stable quasi-D_{6h} Dy(III) single-molecule magnets, the first of their kind, are reported. A comparison of complexes **1** and **2** leads to the conclusion that QTM is highly dependent on the local symmetries of the crystal field. The calculation results of the designed nearly ideal hexagonal bipyramidal Dy model complex with 18-crown-6 has a much stronger magnetic anisotropy than **1** and **2**. When the ground Kramers doublet of the metal ions is more axial, QTM will be suppressed more effectively. From these results, it can be concluded that the crystal field produced by a hexagonal bipyramidal geometry is a viable crystal field for designing high performance SMMs. Moreover, the work illustrates how controlling crystal morphology can effectively tune the symmetries of the crystal field. Slight changes in crystal field triggered by crystallographic packing effects provide a means for more deeply understanding magneto-structural correlations and the mechanisms of slow magnetic relaxation. Ongoing efforts in our laboratory aimed at obtaining a high performance SMM in a perfect hexagonal bipyramidal geometry are underway.

EXPERIMENTAL SECTION

General Methods. All reagents and solvents were purchased from commercial sources without any purification. The ligand *t*-Bu_3PO was prepared by a reported procedure.[21]

Preparation of $Dy(NO_3)_3(t\text{-}Bu_3PO)_2$ (1). $Dy(NO_3)_3{\cdot}6H_2O$ (55 mg, 0.12 mmol) in 5 mL of EtOH and *t*-Bu_3PO (55 mg, 0.25 mg) in 5 mL of EtOH were mixed and stirred for 10 min. The solution was evaporated slowly over the course of a month to give white block single crystals of **1** with a yield of 81% based on Dy. Elemental analysis calcd (%) for $C_{24}H_{54}DyN_3O_{11}P_2$: C (36.71), N (5.35), H (6.93); found: C (36.57), N (5.20), H (6.82). IR data ATR (cm^{-1}): 1514(m), 1467(s), 1272(s), 1022(s) for NO; 1055(s) for P═O.

Preparation of $Dy(NO_3)_3(t\text{-}Bu_3PO)_2{\cdot}0.5CH_3CN$ (2). $Dy(NO_3)_3{\cdot}6H_2O$ (55 mg, 0.12 mmol) in 5 mL of CH_3CN and *t*-Bu_3PO (55 mg, 0.25 mg) in 5 mL of CH_3CN were mixed and stirred for 10 min. The solution was evaporated slowly over the course of a month to give white block shaped single crystals of **2** in a 92% yield based on Dy. Elemental analysis calcd (%) for $C_{50}H_{111}Dy_2N_7O_{22}P_4$: C (37.26), N (6.08), H (6.94); found: C (37.37), N (5.98), H (6.85). IR data ATR (cm^{-1}): 1517(m), 1465(s), 1272(s), 1023(s) for NO; 1053(s) for P═O.

Crystallographic Data Collection and Refinement. Crystallographic data of complexes **1** and **2** were collected on a Bruker APEX-II CCD area-detector diffractometer with Mo Kα radiation (λ = 0.71073 Å) using an φ and ω scans at 296 K. The diffraction data were integrated using SAINT,[30a] and were corrected for absorption using SADABS.[30b] All non-hydrogen atoms were located by the Patterson method.[30c] The structures were solved by direct methods and refined using the full-matrix least-squares technique within the SHELXTL program package.[30d] All non-hydrogen atoms were refined with anisotropic displacement parameters. The hydrogen atoms were generated geometrically (C−H 0.96 Å) using the riding-model. CCDC 1520163 and 1491580 contain the supplementary crystallographic data for this paper. These data can be obtained free of charge from The Cambridge Crystallographic Data Centre via www.ccdc.cam.ac.uk/data_request/cif.

Physical Measurements. The IR spectra were carried out using a Nexus 870 FT-IR spectrometer with KBr pellets in the range from 400 to 4000 cm^{-1}. Elemental analyses of C, N, and H were measured on a PerkinElmer 240C elemental analyzer. The static magnetic measurements were collected on a MPMS-XL7 SQUID magnetometer. The alternating current (ac) susceptibility measurements were collected on a Quantum Design VSM SQUID magnetometer. The static magnetic measurements were performed in the temperature range 1.8−300 K in a field of 1000 Oe and the magnetization isothermal measurements were performed in fields of between 0 and 7 T on a polycrystalline sample. The ac susceptibility measurements were carried out under an oscillating field of 2 Oe with frequency ranging from 1 to 999 Hz. Experimental susceptibilities were corrected for diamagnetism using Pascal's constants[31] and for the sample holder by previous calibration.

***Ab Initio* Calculations for Complexes 1, 2, and Model Complex.** Complete-active-space self-consistent field (CASSCF) calculations on the Dy fragments (see Figure S18) of complexes **1** and **2** on the basis of X-ray data were carried out with the MOLCAS 8.2 program package.[26] The model complex is based on $[Nd(18\text{-crown-}6)(BH_4)_2]^+$.[32] For CASSCF calculations, the basis sets for all atoms are atomic natural orbitals from the MOLCAS ANO-RCC library: ANO-RCC-VTZP for Dy(III) ion; VTZ for close O; VDZ for distant atoms. The calculations employed the second order Douglas−Kroll−Hess Hamiltonian,[33] where scalar relativistic contractions were taken into account in the basis set and the spin−orbit coupling was handled separately in the restricted active space state interaction (RASSI-SO) procedure.[34] The active electrons in 7 active spaces include all f electrons CAS (9 in 7) for three complexes in the CASSCF calculation. To exclude all doubts we calculated all the roots in the active space. The maximum number of spin-free states that were possible with our hardware included all from 21 sextets, 128 from 224 quadruplets, and 130 from 490 doublets for Dy(III) fragments.

ASSOCIATED CONTENT

Supporting Information

are in Supporting Information. This material is available free of charge on the ACS Publications Web site The Supporting Information is available free of charge on the ACS Publications website at DOI: 10.1021/acs.inorgchem.8b03206.

Full experimental and crystallographic details (PDF)

Accession Codes

CCDC 1491580 and 1520163 contain the supplementary crystallographic data for this paper. These data can be obtained free of charge via www.ccdc.cam.ac.uk/data_request/cif, or by emailing data_request@ccdc.cam.ac.uk, or by contacting The Cambridge Crystallographic Data Centre, 12 Union Road, Cambridge CB2 1EZ, UK; fax: +44 1223 336033.

AUTHOR INFORMATION

Corresponding Authors

*E-mail: zhangyiquan@njnu.edu.cn.
*E-mail: yousong@nju.edu.cn.
*E-mail: dunbar@chem.tamu.edu.

ORCID

Brian S. Dolinar: 0000-0002-8228-4590
Fei Yu: 0000-0001-9721-271X
Yi-Quan Zhang: 0000-0003-1818-0612
You Song: 0000-0002-0289-7830
Kim R. Dunbar: 0000-0001-5728-7805

DOI: 10.1021/acs.inorgchem.8b03206
Inorg. Chem. 2019, 58, 2610−2617

Notes

The authors declare no competing financial interest.

■ ACKNOWLEDGMENTS

This work was supported by the Major State Basic Research Development Program (2017YFA0303203 and 2018YFA0306004), National Natural Science Foundation of China (91622115 and 21571097), Natural Science Foundation of Jiangsu Province of China (BK20151542), Specialized Research Fund for the Doctoral Program of Higher Education supported by Nanjing University Innovation and Creative Program for PhD candidate CXCY17-20. KRD is grateful to the National Science Foundation (CHE-1808779) and the Robert A. Welch Foundation (A-1449) for support of this work.

■ REFERENCES

(1) Sessoli, R.; Gatteschi, D.; Caneschi, A.; Novak, M. A. Magnetic bistability in a metal-ion cluster. *Nature* **1993**, *365*, 141.

(2) Tejada, J.; Chudnovsky, E. M.; del Barco, E.; Hernandez, J. M.; Spiller, T. P. Magnetic qubits as hardware for quantum computers. *Nanotechnology* **2001**, *12*, 181.

(3) (a) Wernsdorfer, W.; Sessoli, R. Quantum Phase Interference and Parity Effects in Magnetic Molecular Clusters. *Science* **1999**, *284*, 133. (b) Leuenberger, M. N.; Loss, D. Quantum computing in molecular magnets. *Nature* **2001**, *410*, 789.

(4) Sessoli, R.; Tsai, H. L.; Schake, A. R.; Wang, S.; Vincent, J. B.; Folting, K.; Gatteschi, D.; Christou, G.; Hendrickson, D. N. High-spin molecules: $[Mn_{12}O_{12}(O_2CR)_{16}(H_2O)_4]$. *J. Am. Chem. Soc.* **1993**, *115*, 1804.

(5) (a) Kostakis, G. E.; Ako, A. M.; Powell, A. K. Structural motifs and topological representation of Mn coordination clusters. *Chem. Soc. Rev.* **2010**, *39*, 2238. (b) Demir, S.; Jeon, I.-R.; Long, J. R.; Harris, T. D. Radical ligand-containing single-molecule magnets. *Coord. Chem. Rev.* **2015**, *289*, 149. (c) Escuer, A.; Esteban, J.; Perlepes, S. P.; Stamatatos, T. C. The bridging azido ligand as a central "player" in high-nuclearity 3d-metal cluster chemistry. *Coord. Chem. Rev.* **2014**, *275*, 87.

(6) (a) Jeon, I.-R.; Park, J. G.; Xiao, D. J.; Harris, T. D. An azophenine radical-bridged Fe2 single-molecule magnet with record magnetic exchange coupling. *J. Am. Chem. Soc.* **2013**, *135*, 16845. (b) Ako, A. M.; Hewitt, I. J.; Mereacre, V.; Clérac, R.; Wernsdorfer, W.; Anson, C. E.; Powell, A. K. A ferromagnetically coupled Mn_{19} aggregate with a record = 83/2 ground spin state. *Angew. Chem., Int. Ed.* **2006**, *45*, 4926.

(7) (a) Neese, F.; Pantazis, D. A. What is not required to make a single molecule magnet. *Faraday Discuss.* **2011**, *148*, 229. (b) Waldmann, O. A criterion for the anisotropy barrier in single-molecule magnets. *Inorg. Chem.* **2007**, *46*, 10035.

(8) (a) Latendresse, T. P.; Vieru, V.; Wilkins, B. O.; Bhuvanesh, N. S.; Chibotaru, L. F.; Nippe, M. Magnetic Properties of a Terbium-[1]Ferrocenophane Complex: Analogies between Lanthanide-Ferrocenophane and Lanthanide-Bis-phthalocyanine Complexes. *Angew. Chem., Int. Ed.* **2018**, *57*, 8164. (b) Ishikawa, N.; Sugita, M.; Ishikawa, T.; Koshihara, S.; Kaizu, Y. Lanthanide double-decker complexes functioning as magnets at the single-molecular level. *J. Am. Chem. Soc.* **2003**, *125*, 8694.

(9) (a) Chen, Y.-C.; Liu, J.-L.; Ungur, L.; Liu, J.; Li, Q.-W.; Wang, L.-F.; Ni, Z.-P.; Chibotaru, L. F.; Chen, X.-M.; Tong, M.-L. Symmetry-Supported Magnetic Blocking at 20 K in Pentagonal Bipyramidal Dy(III) Single-Ion Magnets. *J. Am. Chem. Soc.* **2016**, *138*, 2829. (b) Liu, J.; Chen, Y.-C.; Liu, J.-L.; Vieru, V.; Ungur, L.; Jia, J.-H.; Chibotaru, L. F.; Lan, Y.; Wernsdorfer, W.; Gao, S.; Chen, X.-M.; Tong, M.-L. A Stable Pentagonal Bipyramidal Dy(III) Single-Ion Magnet with a Record Magnetization Reversal Barrier over 1000 K. *J. Am. Chem. Soc.* **2016**, *138*, 5441. (c) Guo, F.-S.; Day, B. M.; Chen, Y.-C; Tong, M.-L.; Mansikkamäki, A.; Layfield, R. A. A Dysprosium Metallocene Single-Molecule Magnet Functioning at the Axial Limit. *Angew. Chem., Int. Ed.* **2017**, *56*, 11445. (d) Goodwin, C. A. P.; Ortu, F.; Reta, D.; Chilton, N. F.; Mills, D. P. Molecular magnetic hysteresis at 60 K in dysprosocenium. *Nature* **2017**, *548*, 439. (e) Meng, Y.-S.; Xu, L.; Xiong, J.; Yuan, Q.; Liu, T.; Wang, B.-W.; Gao, S. Low-Coordinate Single-Ion Magnets by Intercalation of Lanthanides into a Phenol Matrix. *Angew. Chem., Int. Ed.* **2018**, *57*, 4673.

(10) (a) Jiang, S.-D.; Wang, B.-W.; Sun, H.-L.; Wang, Z.-M.; Gao, S. An organometallic single-ion magnet. *J. Am. Chem. Soc.* **2011**, *133*, 4730. (b) Ungur, L.; Le Roy, J. J.; Korobkov, I.; Murugesu, M.; Chibotaru, L. F. Fine-tuning the local symmetry to attain record blocking temperature and magnetic remanence in a single-ion magnet. *Angew. Chem., Int. Ed.* **2014**, *53*, 4413. (c) Meihaus, K. R.; Long, J. R. Magnetic blocking at 10 K and a dipolar-mediated avalanche in salts of the bis(η^8-cyclooctatetraenide) complex $[Er(COT)_2]^-$. *J. Am. Chem. Soc.* **2013**, *135*, 17952. (d) Zhang, P.; Zhang, L.; Wang, C.; Xue, S.; Lin, S.-Y.; Tang, J. Equatorially coordinated lanthanide single ion magnets. *J. Am. Chem. Soc.* **2014**, *136*, 4484.

(11) (a) Craig, G. A.; Murrie, M. 3d single-ion magnets. *Chem. Soc. Rev.* **2015**, *44*, 2135. (b) Bar, A. K.; Pichon, C.; Sutter, J.-P. Magnetic anisotropy in two- to eight-coordinated transition−metal complexes: Recent developments in molecular magnetism. *Coord. Chem. Rev.* **2016**, *308*, 346.

(12) (a) Gómez-Coca, S.; Aravena, D.; Morales, R.; Ruiz, E. Large magnetic anisotropy in mononuclear metal complexes. *Coord. Chem. Rev.* **2015**, *289-290*, 379. (b) Feng, M.; Tong, M.-L. Single Ion Magnets from 3d to 5f: Developments and Strategies. *Chem. - Eur. J.* **2018**, *24*, 7574.

(13) Gatteschi, D.; Sessoli, R. Quantum tunneling of magnetization and related phenomena in molecular materials. *Angew. Chem., Int. Ed.* **2003**, *42*, 268.

(14) Liu, J.-L.; Chen, Y.-C.; Tong, M.-L. Symmetry strategies for high performance lanthanide-based single-molecule magnets. *Chem. Soc. Rev.* **2018**, *47*, 2431.

(15) (a) Le Roy, J. J.; Ungur, L.; Korobkov, I.; Chibotaru, L. F.; Murugesu, M. Coupling strategies to enhance single-molecule magnet properties of erbium-cyclooctatetraenyl complexes. *J. Am. Chem. Soc.* **2014**, *136*, 8003. (b) Zhang, Y.-Q.; Luo, C.-L.; Wang, B.-W.; Gao, S. Understanding the magnetic anisotropy in a family of N_2^{3-} radical-bridged lanthanide complexes: density functional theory and ab initio calculations. *J. Phys. Chem. A* **2013**, *117*, 10873. (c) Li, J.; Wei, R.-M.; Pu, T.-C.; Cao, F.; Yang, L.; Han, Y.; Zhang, Y.-Q.; Zuo, J.-L.; Song, Y. Tuning quantum tunnelling of magnetization through 3d−4f magnetic interactions: an alternative approach for manipulating single-molecule magnetism. *Inorg. Chem. Front.* **2017**, *4*, 114.

(16) Chen, Y.-C.; Liu, J.-L.; Wernsdorfer, W.; Liu, D.; Chibotaru, L. F.; Chen, X.-M.; Tong, M.-L. Hyperfine-Interaction-Driven Suppression of Quantum Tunneling at Zero Field in a Holmium(III) Single-Ion Magnet. *Angew. Chem., Int. Ed.* **2017**, *56*, 4996.

(17) (a) Görller-Walrand, C.; Binnemans, K. *Handbook on the Physics and Chemistry of Rare Earths* **1996**, *23*, 121. (b) Stevens, K. W. H. Matrix Elements and Operator Equivalents Connected with the Magnetic Properties of Rare Earth Ions. *Proc. Phys. Soc., London, Sect. A* **1952**, *65*, 209. (c) Bleaney, B.; Stevens, K. W. H. Paramagnetic resonance. *Rep. Prog. Phys.* **1953**, *16*, 108.

(18) (a) Yao, X.-N.; Du, J.-Z.; Zhang, Y.-Q.; Leng, X.-B.; Yang, M.-W.; Jiang, S.-D.; Wang, Z.; Ouyang, Z.-W.; Deng, L.; Wang, B.-W.; Gao, S. Two-Coordinate Co(II) Imido Complexes as Outstanding Single-Molecule Magnets. *J. Am. Chem. Soc.* **2017**, *139*, 373. (b) Zadrozny, J. M.; Xiao, D. J.; Atanasov, M.; Long, G. J.; Grandjean, F.; Neese, F.; Long, J. R. Magnetic blocking in a linear iron(I) complex. *Nat. Chem.* **2013**, *5*, 577.

(19) Wu, J.; Jung, J.; Zhang, P.; Zhang, H.; Tang, J.; Le Guennic, B. *Cis-trans* isomerism modulates the magnetic relaxation of dysprosium single-molecule magnets. *Chem. Sci.* **2016**, *7*, 3632.

(20) Li, Q.-W.; Wan, R.-C.; Chen, Y.-C.; Liu, J.-L.; Wang, L.-F.; Jia, J.-H.; Chilton, N. F.; Tong, M.-L. Unprecedented hexagonal bipyramidal single-ion magnets based on metallacrowns. *Chem. Commun.* **2016**, *52*, 13365.

DOI: 10.1021/acs.inorgchem.8b03206
Inorg. Chem. 2019, 58, 2610−2617

(21) Bowden, A.; Coles, S. J.; Pitak, M. B.; Platt, A. W. G. Complexes of lanthanide nitrates with tri tert butylphosphine oxide. *Inorg. Chem.* **2012**, *51*, 4379.
(22) Alvarez, S.; Avnir, D.; Llunell, M.; Pinsky, M. Continuous symmetry maps and shape classification. The case of six-coordinated metal compounds. *New J. Chem.* **2002**, *26*, 996.
(23) Guo, Y. N.; Xu, G. F.; Guo, Y.; Tang, J. Relaxation dynamics of dysprosium(III) single molecule magnets. *Dalton Trans.* **2011**, *40*, 9953.
(24) Shrivastava, K. N. Theory of Spin−Lattice Relaxation. *Phys. Status Solidi B* **1983**, *117*, 437.
(25) Abragam, A.; Bleaney, B. *Electron Paramagnetic Resonance of Transition Ions*; Oxford University Press: Oxford, U.K., 2012.
(26) Karlstrom, G.; Lindh, R.; Malmqvist, P. A.; Roos, B. O.; Ryde, U.; Veryazov, V.; Widmark, P. O.; Cossi, M.; Schimmelpfennig, B.; Neogrady, P.; Seijo, L. MOLCAS: a program package for computational chemistry. *Comput. Mater. Sci.* **2003**, *28*, 222.
(27) (a) Garanin, D. A.; Chudnovsky, E. M. Thermally activated resonant magnetization tunneling in molecular magnets: Mn_{12}Ac and others. *Phys. Rev. B: Condens. Matter Mater. Phys.* **1997**, *56*, 11102. (b) Leuenberger, M. N.; Loss, D. Spin tunneling and phonon-assisted relaxation in Mn_{12}-acetate. *Phys. Rev. B: Condens. Matter Mater. Phys.* **2000**, *61*, 1286.
(28) Ungur, L.; Thewissen, M.; Costes, J.-P.; Wernsdorfer, W.; Chibotaru, L. F. Interplay of strongly anisotropic metal ions in magnetic blocking of complexes. *Inorg. Chem.* **2013**, *52*, 6328.
(29) (a) Lunghi, A.; Totti, F.; Sessoli, R.; Sanvito, S. The role of anharmonic phonons in under-barrier spin relaxation of single molecule magnets. *Nat. Commun.* **2017**, *8*, 14620. (b) Lunghi, A.; Totti, F.; Sanvito, S.; Sessoli, R. Intra-molecular origin of the spin-phonon coupling in slow-relaxing molecular magnets. *Chem. Sci.* **2017**, *8*, 6051. (c) Tesi, L.; Lunghi, A.; Atzori, M.; Lucaccini, E.; Sorace, L.; Totti, F.; Sessoli, R. Giant spin-phonon bottleneck effects in evaporable vanadyl-based molecules with long spin coherence. *Dalton Trans.* **2016**, *45*, 16635.
(30) (a) *SAINT* v5.0−6.01; Bruker Analytical X-ray Systems Inc.: Madison, WI, 1998. (b) Sheldrick, G. M. *SADABSs: An Empirical Absorption Correction Program*; Bruker Analytical X-ray Systems Inc.: Madison, WI, 1996. (c) Patterson, A. L. A Fourier Series Method for the Determination of the Components of Interatomic Distances in Crystals. *Phys. Rev.* **1934**, *46*, 372. (d) *SHELXTL* 6.10; Bruker Analytical Instrumentation: Madison, WI, 2000.
(31) Bain, G. A.; Berry, J. F. Diamagnetic Corrections and Pascal's Constants. *J. Chem. Educ.* **2008**, *85*, 532.
(32) Arliguie, T.; Belkhiri, L.; Bouaoud, S.-E.; Thuéry, P.; Villiers, C.; Boucekkine, A.; Ephritikhine, M. Lanthanide(III) and Actinide(III) Complexes $[M(BH_4)_2(THF)_5][BPh_4]$ and $[M(BH_4)_2$(18-crown-6)$][BPh_4]$ (M = Nd, Ce, U): Synthesis, Crystal Structure, and Density Functional Theory Investigation of the Covalent Contribution to Metal-Borohydride Bonding. *Inorg. Chem.* **2009**, *48*, 221.
(33) Sandhoefer, B.; Neese, F. One-electron contributions to the g-tensor for second-order Douglas−Kroll−Hess theory. *J. Chem. Phys.* **2012**, *137*, 094102.
(34) Sánchez-Sanz, G.; Barandiarán, Z.; Seijo, L. Energy level shifts in two-step spin−orbit coupling ab initio calculations. *Chem. Phys. Lett.* **2010**, *498*, 226.

DOI: 10.1021/acs.inorgchem.8b03206
Inorg. Chem. 2019, 58, 2610−2617